A comparison of wrist MRI at 3T and 7T using adjustable receiver arrays

J. A. Nordmeyer-Massner[1], M. Wyss[1], G. Andreisek[2], J. Hodler[3], and K. P. Pruessmann[1]

[1]Institute for Biomedical Engineering, University and ETH Zurich, Zurich, Switzerland, [2]Institute for Diagnostic Radiology, University Hospital Zurich, Zurich, Switzerland, [3]Departement of Radiology, Balgrist University Hospital, Zurich, Switzerland

Introduction The human wrist comprises a lot of small but clinically important structures. In order to resolve these structures the signal-to-noise ratio (SNR) must be maximized. It has previously been shown at 3T that mechanical adjustability benefits the SNR performance of coil arrays by bringing the coil elements very close to the individual anatomy of interest [1]. From even higher magnetic field strengths such as 7T a further gain in SNR may be expected. The aim of the present work was to study the actual SNR benefit of going from 3T to 7T in wrist imaging. The basis for this comparison is the use of custom-built, geometrically identical 8-channel wrist arrays for both field strengths, building on the existing 3T design [1]. Using these arrays the dominant wrists of 10 healthy volunteers were scanned, permitting a quantitative SNR comparison for several anatomical regions of interest (ROI).

Materials and Methods The 7T array (Fig. 1) is similar to the 3T version presented in Ref. [1]. It consists of 8 trapezoidal coil elements. Designed for receive-only operation, the array had to be fitted into an available volume transmit coil, prompting the slightly different layout of the acrylic frame. Coaxial cables of 20 cm in length connect the coil elements to a multiple-channel interface box that contains a low-noise preamplifier for each channel and provides connection to the spectrometer. 7T data were acquired on a Philips Achieva system (Philips Healthcare, Cleveland, Ohio, USA), using a gradient echo sequence (FOV 80 mm, TE 9 ms, TR 204 ms, 320 x 320 acq. matrix, NSA 4, slice thickness 2 mm, 15 slices, 4:20 min) in both coronal and transverse slice orientation. All measurements included a noise scan without signal excitation to assess the noise covariance matrix $\boldsymbol{\Psi}$ of the array with great accuracy. The same procedures and sequence parameters were used to acquire corresponding data on a 3T Philips Achieva system (Philips Healthcare, Best, The Netherlands) for comparison. For SNR analysis the image data were modeled on a pixel-by-pixel basis as shown in Eq. (1). Here $\boldsymbol{d}$ denotes a vector containing the complex values that the different coils yield for a given pixel, ρ and $\boldsymbol{s}$ denote the exact value of the available transverse magnetization and a vector containing the complex-valued sensitivities of the array elements at this position, respectively, and the vector $\boldsymbol{\eta}$ reflects the thermal noise components. According to Ref. [2] the optimum-SNR estimate of ρ, $\hat{\rho}$ is then given by Eq. (2) and the variance of its noise component by Eq. (3). On this basis the SNR of the combined pixel value can be calculated according to Eq. (4), which requires knowledge only of the complex single-coil image data and the equally measured noise statistics $\boldsymbol{\Psi}$. The resulting SNR was analyzed in several regions of interest (ROI) in the cartilages of several carpal bones, the trabecular bone in the lunatum, and the triangular fibrocartilage complex (TFCC) in the coronal slices, as well as in the median nerve in a transverse slice at the level of the pisiforme. Figure 2 shows a sample coronal SNR map along with indications of the eight ROIs that were hand-drawn in each data set. Within these ROIs the SNR was averaged. Furthermore the images were qualitatively scored by two independent radiologists based on criteria similar to those described in Ref. [4].

$$\boldsymbol{d} = \boldsymbol{s}\rho + \boldsymbol{\eta} \quad (1)$$

$$\hat{\rho} = \left(\boldsymbol{s}^H \boldsymbol{\Psi}^{-1} \boldsymbol{s}\right)^{-1} \boldsymbol{s}^H \boldsymbol{\Psi}^{-1} \boldsymbol{d} \quad (2)$$

$$\sigma^2 = \left(\boldsymbol{s}^H \boldsymbol{\Psi}^{-1} \boldsymbol{s}\right)^{-1} \quad (3)$$

$$SNR = \frac{|\rho|}{\left(\boldsymbol{s}^H \boldsymbol{\Psi}^{-1} \boldsymbol{s}\right)^{-\frac{1}{2}}} = \sqrt{\rho^* \boldsymbol{s}^H \boldsymbol{\Psi}^{-1} \boldsymbol{s} \rho} \approx \sqrt{\boldsymbol{d}^H \boldsymbol{\Psi}^{-1} \boldsymbol{d}} \quad (4)$$

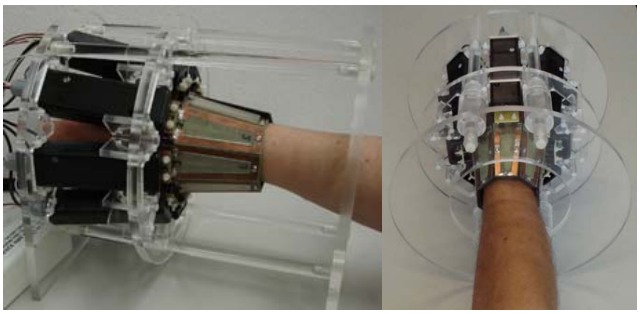

Fig. 1: The 8-channel wrist coil array for 3T (left) and 7T (right) closed around a volunteer's wrist. The coil arrays are geometrically identical.

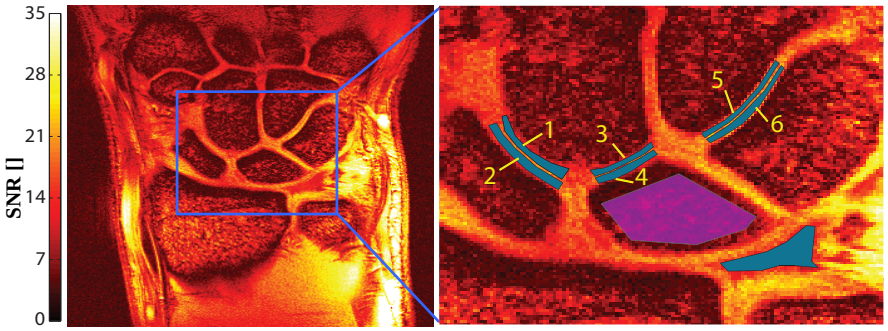

Fig. 2: Quantitative SNR map of a coronal slice. The blue ROIs 1-6 are placed in cartilage layers, the bottom blue ROI measures SNR in the TFCC and the purple ROI in the trabecular bone structure of the lunatum.

Results The results of the SNR analysis are shown in Tab. 1, listing the mean SNR and its standard deviation across the volunteers. At 3T all 10 data sets were suitable for evaluation, while 3 of the 7T data sets were discarded as outliers with SNR deviations of more than two times the standard deviation. In two cases the underlying problem was incomplete adjustment of the coil array to particularly large wrists. In the third case the transmit resonator was wrongly positioned. As the numbers in Tab. 1 indicate a significant SNR gain was observed in all structures except trabecular bone. In several structures the SNR was approximately doubled at 7T. However, the qualitative analysis revealed no significant difference between the two field strengths with respect to the visibility of anatomical structures ($p = 0.72$ and $p = 0.65$ for reader 1 and 2, respectively), with a kappa value of 0.71 indicating substantial [5] interobserver agreement.

Discussion According to this study, 7T offers up to about twice as much sensitivity as 3T in wrist imaging. However, the SNR gain varies substantially between different structures and types of tissue, indicating the influence of tissue-dependent factors such as relaxation and short-range field inhomogeneity. In trabecular bone, particularly, no SNR gain was observed, which is most likely due to much shorter T2* at 7T. The qualitative assessment by the two readers indicates that the general SNR benefit did not translate into a palpable increase in image information. This paradox remains to be further investigated. One factor may be increased T2* blurring and fat-shift in the 7T data, as well as the fact that the RF coverage was not quite as homogeneous as at 3T due to increased tissue interaction. All of these issues call for field-strength-dependent protocol optimization. In addition the confirmed SNR gain at 7T could potentially be better leveraged by targeting yet higher spatial resolution or accelerating the exam by performing fewer averages.

References [1]Massner et al., Proc. ISMRM, p. 416 (2006) [2] Roemer et al., MRM 16, p.192 (1990) [3] Pruessmann et al., MRM 46, p.638 (2001) [4] Saupe et al., Radiology 234, p.256 (2005) [5] Landis et al., Biometrics 33, p.159(1977)

	Lunatum	Cartilage 1	Cartilage 2	Cartilage 3	Cartilage 4	Cartilage 5	Cartilage 6	TFCC	Median Nerve
3T	6.45 ± 0.58	19.57 ± 2.49	20.79 ± 1.29	18.07 ± 1.58	17.99 ± 1.97	17.79 ± 1.79	18.42 ± 2.03	10.77 ± 2.04	20.66 ± 2.40
7T	6.39 ± 0.72	28.42 ± 2.69	28.13 ± 1.29	24.49 ± 5.00	22.91 ± 6.38	35.62 ± 7.57	35.80 ± 6.24	21.24 ± 3.17	39.97 ± 17.04

Table 1: SNR in selected anatomical structures. The numbers of the cartilage ROIs correspond to the numbers shown in Fig. 2.